Pergamon

Int. J. Heat Mass Transfer. Vol. 40, No. 8, pp. 1963–1976, 1997

0017–9310/97 $17.00 + 0.00

PII: S0017-9310(96)00237-2

Homogeneous turbulence evolution in stably stratified flow—II. Asymptotic regimes of large evolution time at low inverse Froude numbers

V. A. BABENKO

The Luikov Heat and Mass Transfer Institute of the Academy of Science, Minsk, Belarus

(*Received* 23 *February* 1995)

Abstract—An attempt has been undertaken to explain and describe, analytically, many of the features of recent experiments and numerical calculations of the homogeneous turbulence evolution in media stratified on density or temperature. Applying various variants of a small parameter method, let us analyze a set of asymptotic regimes of turbulent velocity and scalar fields development in the final stage of turbulence decay.

1. INTRODUCTION

In a number of experimental and theoretical works, analyzing grid-generated turbulence decaying in a stably stratified fluid, the periodic oscillations of the convective vertical mass flux were detected, as well as the oscillations of squared velocity and scalar fluctuations. These oscillations produced by buoyancy forces can be treated as internal gravity waves in turbulent flow. At some conditions internal waves can interchange their kinetic and potential energy with irregular turbulent motion radically changing the rate and character of turbulence decay. One can find a brief review of works dealing with the problem in refs. [1–6].

This paper represents the second part of our study aimed at analytical and semi-analytical investigation of the second-order turbulence model developed earlier in ref. [7] and applied to the problem of stably stratified grid-generated turbulence in ref. [5]. Paper [5] numerically studied homogeneous turbulence horizontally propagated in vertically stratified media. The results were found to accord with previously obtained ones in experiments by Itswier *et al.* [4], in a salt water tank and by Lienhard *et al.* [2], in an air wind tunnel.

Here, as well as in the first part of current work, [6], an analytical study of stratified homogeneous turbulence is carried out on the basis of the same model as in ref. [5] and with the same initial conditions. It allows us to compare the results thoroughly. Analytical treatment of the problem lets us describe the specific features of stratified turbulence more clearly. On the other hand, naturally, only those features that the theory itself contains, [7], can be obtained this way.

In the first part of the paper, [6], with a small parameter decomposition on an inverse Froude number using the multiple scale method (see, for instance ref. [8]), the basic set of governing equations was split into subsystems describing non-linear internal waves and wave averaged behavior of turbulence. The phase and frequency of internal gravity waves and relations between amplitudes were obtained in ref. [6] explicitly, while the rest of the parameters (wave averaged functions and amplitude of vertical mass flux) were to be found numerically, on the ground of a more simple equation set. The aim of this paper is to find out the analytical solutions for this second group of parameters in the asymptotic case of weak turbulence (final stage of turbulence decay) discussing the interaction of internal waves and active turbulence.

2. FINAL STAGE ANALYSIS

In this chapter we shall consider a final stage of turbulence decay at $\tau \to \infty$ and $R_\lambda \ll 1$. The condition $R_\lambda \ll 1$ means the *weak turbulence*, that is the turbulence with negligible inertia. Later, in another paper we shall discuss the possibility of turbulence Reynolds number *not being small* in a final stage of turbulence decay.

Earlier in ref. [6] it was shown that at large distances downstream the turbulence source (distant area) the evolution of stratified turbulence can be considered as a singular problem in a sense of small parameter methods (see, for instance ref. [11]), because the differential order of the model is lowered. In distant and final areas (in our analysis the latter is a partial case of the former at $\tau \to \infty$) the equation for convective mass flux, $\hat{q}$, degenerates into an algebraic

NOMENCLATURE

$E = \overline{u_i^2}/U^2$ dimensionless kinetic energy
$F = NM/U$ inverse Froude number
$K = \overline{u_2^2}/u_i^2$ anisotropy coefficient
M cell size of a grid
$N = (g\,\mathrm{d}\bar{\rho}/\bar{\rho}\,\mathrm{d}x_2)^{1/2}$ Brunt–Väisälä
$Q = (\overline{-u_2\rho})/(UM^{\mathrm{d}\bar{\rho}}/\mathrm{d}x_2)$ dimensionless vertical turbulent mass flux
$R_\lambda = (5ET_uRe)^{1/2}$ turbulence Reynolds number
$Re = UM/\nu$ Reynolds number
$T_u = (\overline{u_i^2}U)/(\varepsilon_u M)$ time scale of velocity field
$T_\rho = (\overline{\rho^2}U)/(\varepsilon_\rho M)$ time scale of density field
U flow velocity
$\overline{u_i^2}$ doubled turbulence kinetic energy (TKE).

Greek symbols
$\varepsilon = F^2$ small parameter
ε_ρ rate of dissipation of density fluctuation
ε_u rate of dissipation of velocity fluctuation
σ molecular Prandtl number
$\tau = \tau^* U/M$ dimensionless time
τ^* dimensional time
$\hat{\tau}$ $\sqrt{\varepsilon}\tau$, $t = \varepsilon T_\rho$
$\Theta = \overline{\rho^2}/(M^{\mathrm{d}\bar{\rho}}/\mathrm{d}x_2)^2$ squared density fluctuation.

form ($\hat{A} = 0$, where $\hat{A} = \hat{K} + \hat{\vartheta}(\hat{d}(\hat{K} - 1/3) - 2/3)$ [6]), which is maintained with a great degree of accuracy.

In theory [7] the dimensionless parameter $d(R_\lambda^2) = 1 - 2/(1 + \sqrt{1 + 2800/R_\lambda^2})$ is equal to $d = 0$ for asymptotically strong turbulence, $R_\lambda \gg 1$, and to $d = 1$ for asymptotically weak turbulence, $R_\lambda \ll 1$, describing the influence of turbulence inertia effects. In the approach of asymptotically weak turbulence at $d \to 1$, and $\tau \gg 1$ the set of differential equations of the model (see system (9) from ref. [6]) can be written in more simple form as

$$\begin{aligned}
\frac{4}{5}\frac{t}{R_\infty}\frac{\mathrm{d}\hat{K}}{\mathrm{d}t} &= -\frac{7\hat{d}'(\hat{K} - 1/3)}{\hat{R}} + 2\hat{q}(\hat{K} - 4/5),\\
\frac{4}{5}\frac{t}{R_\infty}\frac{\mathrm{d}\hat{R}}{\mathrm{d}t} &= \frac{4}{5}(1 - \hat{R}/R_\infty) - 2(1 - \alpha_2\hat{R})\hat{R}\hat{q},\\
0 &= \hat{K} + \hat{\vartheta}(\hat{d}(\hat{K} - 1/3) - 2/3),\\
\frac{4}{5}\frac{t}{R_\infty}\frac{\mathrm{d}\hat{\vartheta}}{\mathrm{d}t} &= 2(\hat{R}^{-1} - 1)\hat{\vartheta} + 2\hat{q}(1 + \hat{\vartheta})\\
\frac{4}{5}\frac{t}{R_\infty}\frac{\mathrm{d}(\hat{d})}{\mathrm{d}t} &= -\frac{d'}{2}\left[-\frac{6/5}{\hat{R}} - 2(2 - \alpha_2\hat{R})\hat{q}\right] \qquad (1)
\end{aligned}$$

where the upper lid denotes the function averaged over internal wave oscillations. In equation (1) function $K = \overline{u_2^2}/\overline{u_i^2}$ represents the part of turbulence kinetic energy (TKE) that is due to vertical fluctuations of velocity, $R = T_u/T_\rho$ is the time scale ratio: $\theta = P/\frac{1}{2}\bar{\rho}u_i^2 = F^2\Theta/E$ is the ratio of potential energy of density fluctuations to TKE, $\alpha_2 = 2d\sigma/(1 + \sigma)(\sigma_\infty + 3/5)$, $d' = 1 - d$, $q = \varepsilon T_\rho Q/E$, $t = \varepsilon T_\rho$. Turbulent Prandtl number σ_∞ and time scale ratio R_∞ at infinity time in a passive scalar case ($F = 0$) are given from the exact analytical solution by ref. [12],

$$\sigma_\infty = \frac{3(1 - \sigma)}{10\sigma}\left[1 - \left(\frac{2\sigma}{1 - \sigma}\right)^{3/2}\right]^{-1}$$

$$R_\infty = \frac{1}{5\sigma}\left[1 - \left(\frac{2\sigma}{1 + \sigma}\right)^{3/2} + \sigma^{3/2}\right] \times \left[1 - 2\left(\frac{2\sigma}{1 + \sigma}\right)^{1/2} + \sigma^{1/2}\right]^{-1}.$$

Let us present the solution of equation (1) as a sum of asymptotic limits (with the index A) and additives (with primes) vanishing at $t \to \infty$ according to power decay laws

$$\hat{f} = f_A + f', \quad f' = C_i t^{-\beta_i}, \quad i = K, R, \theta, q, d \qquad (2)$$

where $\hat{f}$ is one of the functions $\hat{K}$, $\hat{R}$, $\hat{\vartheta}$, $\hat{q}$, $\hat{d}$. All the exponents β_i in (2) should be positive. When the functions $\hat{K}$, $\hat{R}$, $\hat{\vartheta}$, $\hat{q}$, $\hat{d}$ tend to their asymptotic limits, the derivatives in left-hand side of (1) vanish, so the limits can be found from the algebraic system

$$\begin{aligned}
0 &= 2q_A(K_A - 4/5),\\
0 &= (1 - R_A/R_\infty) - 2(1 - \alpha_2 R_A)R_A q_A\\
0 &= K_A + \vartheta_A(K_A - 1),\\
0 &= 2(R_A^{-1} - 1)\vartheta_A + 2q_A(1 + \vartheta_A). \qquad (3)
\end{aligned}$$

The equality in the first equation of system (3) is possible in two cases: (A) at $q_A = 0$; and (B) at $q_A \neq 0$, in the latter case $K_A = 4/5$. We shall also allocate subcases (A1) $q_A = 0$, $\vartheta_A \neq 0$ and (A2) $q_A = 0$, $\vartheta_A = 0$.

In case A1 can find step-by-step from the line of equation (3) marked in parenthesis above the equality sign the following

$$q_A \overset{(1)}{=} 0, \quad R_A \overset{(2)}{=} R_\infty, \quad \vartheta_A \overset{(3)}{=} K_A/(1-K_A), \qquad (4)$$

$$R_A \overset{(4)}{=}, \quad R_\infty \overset{(2),(4)}{=} 1$$

The asymptotic limit K_A remains uncertain. The function $R_\infty(\sigma)$ takes the value $R_\infty = 1$ at the molecular Prandtl number $\sigma = 1$. Hence, case A1 corresponds to the value $\sigma = 1$.

In case A2 we obtain

$$q_A = 0, \quad R_A = R_\infty, \quad K_A = 0, \quad \vartheta_A = 0, \qquad (5)$$

and in case B, respectively,

$$K_A = \tfrac{4}{5}, \quad \vartheta_A = 4, \quad q_A = \tfrac{4}{5}(1-R_A^{-1}), \qquad (6)$$

where R_A is determined as a root of the quadratic equation

$$\alpha_2 R_A^2 - \left(1+\alpha_2+\tfrac{5}{8}\alpha_3\right)R_A + \tfrac{3}{2} = 0 \qquad (7)$$

and $\alpha_3 = 4d/5R_\infty$. The question of which of the roots of equation (7) should be selected and which ranges of the molecular Prandtl number, σ, expressions (5), (6) correspond to, we shall consider later.

To deduce equations for additives let us term-by-term subtract relations (3) from relations (1) and linearize the system for additives, neglecting squared terms. Depending on the case we consider, A1, A2 or B, we get three different systems.

For case A1 the procedure of linearization results in

$$\begin{aligned}
\frac{4}{5}t\frac{dK'}{dt} &= -7d'(K_A-1/3) - 2q'(K_A-4/5)\\
\frac{4}{5}t\frac{dR'}{dt} &= \frac{4}{5}(-R')\\
\frac{4}{5}t\frac{d\vartheta'}{dt} &= -2\vartheta_A R' + 2q'(1+\vartheta_A)\\
0 &= (1+\vartheta_A)K' + \vartheta'(K_A-1) - d'\vartheta_A(K_A-1/3)\\
\frac{4}{5}t\frac{d(d')}{dt} &= -3/5d'.
\end{aligned} \qquad (8)$$

For case A2 it follows

$$\begin{aligned}
\frac{4}{5}\frac{t}{R_\infty}\frac{dK'}{dt} &= \frac{7}{3}\frac{d'}{R_\infty} - \frac{8}{5}q'\\
\frac{4}{5}\frac{t}{R_\infty}\frac{dR'}{dt} &= -\frac{4}{5}R'/R_\infty - 2(1-\alpha_2 R_\infty)R_\infty q'\\
\frac{4}{5}\frac{t}{R_\infty}\frac{d\vartheta'}{dt} &= 2\left(\frac{1}{R_\infty}-1\right)\vartheta' + 2q'\\
0 &= K' - \vartheta',\\
\frac{4}{5}\frac{t}{R_\infty}\frac{d(d')}{dt} &= -\frac{3}{5}\frac{d'}{R_\infty}
\end{aligned} \qquad (9)$$

and, at last, in case B the system for the additives takes the form

$$\begin{aligned}
\frac{4}{5}\frac{t}{R_\infty}\frac{dK'}{dt} &= -\frac{49}{15}d' + \frac{8}{5}(1-R_A^{-1}),\\
\frac{4}{5}\frac{t}{R_\infty}\frac{dR'}{dt} &= -\frac{4}{5}(1-R_A/R_\infty)d'\\
&\quad -\frac{4}{5}(R_\infty^{-1} + 2(1-R_A)(1-2\alpha_2 R_A))R'\\
&\quad -2(1-\alpha_2 R_A)R_A q',\\
\frac{4}{5}\frac{t}{R_\infty}\frac{d\vartheta'}{dt} &= \frac{2}{5}\left(\frac{1}{R_A}-1\right)\vartheta' + 10q' - \frac{8}{R_A^2}R'\\
0 &= 5K' - \vartheta'/5 - \frac{28}{11}d',\\
\frac{4}{5}\frac{t}{R_\infty}\frac{d(d')}{dt} &= \frac{d'}{2}\left[-\frac{6}{5R_A} - 2(2-\alpha_2 R_A)\frac{4}{5}(1-R_A^{-1})\right].
\end{aligned} \qquad (10)$$

Now we shall sequentially consider cases A1, A2 and B, described by systems (8)–(10). Solving these systems, it should be taken into account that these equations are correct approximately, with an accuracy to neglected terms. At $t \to \infty$ the terms rejected are certainly much less than the terms included, however, some of the terms included can also be of a small order depending on the exponents β_i. To investigate the problem we shall carry the asymptotic analysis using the symbols of the order of magnitude, defined as $O(f') = \mathrm{d}(\ln f')/\mathrm{d}\ln t$.

In case A2 the function K' and ϑ' are equivalent, so the ϑ'-function can be excluded from the consideration. It follows from the fifth equation of system (9), that $O(d') = -3/4$. The second equation in system (9) can be solved separately from the system. From the third equation of system (9) we can find out, that $O(K') \geqslant O(q')$, otherwise the function ϑ' would vanish and the system would become over-determined. If a strict inequality $O(K') > O(q')$ takes place, analyzing the first equation we have to recognize, that $O(K') = O(d') = -3/4$, but this order of K' does not correspond to the order of K' in the third equation, $O(K') = O(\vartheta') = 5/2(R_\infty - 1)$. Hence, we have to conclude that $O(K') = O(q')$. The order of magnitude $O(d')$ in the first equation can be less than the order of q' or equal to it, $O(d') \leqslant O(q')$. We shall consider the two variants separately.

Case A2a: $\mathrm{O(K')} = \mathrm{O}(\vartheta') = \mathrm{O(q')} = \mathrm{O(d')} = -3/4$

Substituting the expected form of solution $\vartheta' = K' = c_K t^{-3/4}$, $q' = c_q t^{-3/4}$, $d' = c_d t^{-3/4}$ into the first and third equation of system (9), we determine the ratios of the factors c_K/c_q and c_d/c_q as

$$c_K/c_q = c_\vartheta/c_q = \left(1 - \frac{13}{10R_\infty}\right)^{-1},$$

$$c_d/c_q = -\frac{9}{35}c_K/c_q + \frac{24}{35}R_\infty. \quad (11)$$

From the second equation of system (9) it follows that $O(R') = O(q')$, otherwise $O(R') > O(q')$, and the order $O(R') = -1$ calculated from the second equation of system (9) appears less than the order of magnitude $O(q') = -3/4$, but this assumption is inconsistent. From system (9) we find the ratio c_R/c_q to be

$$c_R/c_q = 10R_\infty^2(1-\alpha_2 R_\infty). \quad (12)$$

The factor c_q remains uncertain.

Case A2b: O(K′) = O(ϑ′) = O1(q′) > O(d′)

In this case the function d' tends to zero at $t \to \infty$ faster than other functions. Replacing ϑ' with K' in equation (3) system (9) and excluding q' from equations (1) and (3) system (9), we obtain

$$O(K') = -\frac{10}{9}(R_\infty - 1). \quad (13)$$

The exponents in power laws are determined by the first equation of system (9)

$$\beta_1 = \frac{10}{9}(R_\infty - 1). \quad (14)$$

From equations (1) and (3), system (9) we find that

$$q' = \tfrac{5}{9}(1-R_\infty^{-1})K'. \quad (15)$$

Substituting the power law expressions with the exponent $-\beta_1$ into system (9), we can find the ratios c_K/c_q, c_R/c_q

$$c_K/c_q = \frac{2}{\beta_1}R_\infty, \quad c_R/c_q = -\frac{5}{2}\frac{(1-\alpha_2 R_\infty)R_\infty}{(1-\beta_1)}. \quad (16)$$

Finishing the consideration of case A2 let us compare the expressions for two of the variants, A2a and A2b. The exponent β_1 should be positive, whence $R_\infty > 1$. On the other hand, the exponent $\beta_1 < \beta_2 = 3/4$, otherwise rejecting the terms with d' in equation (1), system (9) is wrong at large t. At small σ the exponent β_1 is large, $\beta_1 > \beta_2$, so variant A2a is realized. Starting from some value of σ_{T1}, determined by the relation,

$$-\tfrac{10}{9}(R_\infty(\sigma_{T1}) - 1) = -\tfrac{3}{4},$$

variant A2b is realized.

Analysis of cases B and A1 can be made according to the same scheme, so we shall omit the details. In case B two variants are also possible, B1 and B2. In the former

$$O(K') = O(\vartheta') = O(R') = O(q') > O(d'), \quad (17)$$

and in the latter

$$O(K') = O(\vartheta') = O(R') = O(q') = O(d'). \quad (18)$$

In case B1 the exponent can be determined from the first line of system (10), since the function d' disappears from it. Denoting $O(K') = O(\vartheta') = O(R') = O(q') = -\beta_1$, we find out, that

$$\beta_1 = -2R_\infty(1-R_A^{-1}). \quad (19)$$

In case B the asymptotic value of the time scales ratio, R, is determined by the solution of quadratic equation (7). At $d = 1$ the solution of equation (7) has the form

$$R_A = \frac{1}{2\alpha_2} + \frac{1}{2} + \frac{1}{4\alpha_2 R_\infty} \pm \frac{\sqrt{(1+\alpha_2+1/2R_\infty)^2 - 6\alpha_2}}{2\alpha_2} \quad (20)$$

Rearranging the expression for the discriminant D

$$D = (1-\alpha_2+1/2R_\infty)^2 + 2\alpha_2(1/R_\infty - 1),$$

we obtain that $D > 0$, if $R_\infty < 1$, so the case corresponds to the values of R_∞ (σ) < 1 and to $\sigma > 1$.

From the condition $\beta_1 > 0$ it is necessary, that $R_A - 1 < 0$ in equation (19). From equation (20) it follows that

$$2\alpha_2(R_A - 1) = (1-\alpha_2+1/2R_\infty) \pm \sqrt{(1-\alpha_2+1/2R_\infty)^2 + 2\alpha_2(R_\infty^{-1} - 1)} < 0$$

so the root in equation (20) should be taken with a minus sign.

For the second branch, B2, the exponent β_2 is identical for all the functions: $O(K') = O(\vartheta') = O(R') = O(q') = O(d') = -\beta_2$. This exponent can be determined from the equation for d' in equation (10) at $d \to 1$

$$\beta_2 = \frac{R_\infty}{R_A}\left(\frac{3}{4} + (2-\alpha_2 R_A)(R_A - 1)\right).$$

Using equation (7) the expression for β_2 can be written shorter as

$$\beta_2 = R_\infty\left(1 - \frac{1}{2R_\infty} + \frac{1}{4R_A}\right). \quad (21)$$

If this value of β_2 is larger than the value of β_1 from equation (19), the branch B1 is realized, as $O(d') < O(K')$. The condition of the branch B2 validity is given by the inequality $\beta_2 \leqslant \beta_1$ which takes the form $R_A \leqslant 7R_\infty/(12R_\infty - 2)$. At $\sigma \approx 1$ these conditions, as it is easy to see, are not satisfied; at increase of Prandtl number from unity up to the transition value $\sigma_{T2} \approx 1.7$ branch B1 is realized, and from σ_{T2} up to $\sigma = \infty$ branch B2 is valid. For branch B2, as well as for branch B1, $R_A - 1 < 0$. It means that the root of equation (7) should be taken with minus sign.

Substituting the expected power solutions into system (10), we obtain for the ratios of coefficients at the powers:

in case B1:

$$\frac{c_K}{c_q} = -\frac{1}{5(R_A^{-1}-1)}\left[1+\frac{2R_\infty}{R_A[(1-\alpha_2 R_A)^{-1}-2\beta_1]}\right]$$

$$\frac{c_\vartheta}{c_q} = 25\frac{c_K}{c_q}, \quad \frac{c_R}{c_q} = -\frac{5}{2}\frac{R_A R_\infty}{(1-\alpha_2 R_A)^{-1}-2\beta_1}. \qquad (22)$$

in case B2

$$\frac{c_R}{c_q} = \frac{a_4 a_5 - a_3}{a_1 a_5 - a_2 a_3}, \quad \frac{c_d}{c_q} = \frac{a_1 - a_2 a_4}{a_1 a_5 - a_2 a_3},$$

$$\frac{c_K}{c_q} = a_6\frac{c_d}{c_q}, \quad \frac{c_\vartheta}{c_q} = \left(25a_6 - \frac{28}{3}\right)\frac{c_d}{c_q}, \qquad (23)$$

where

$$a_1 = -3+\frac{15}{4R_A}-\frac{1}{2R_\infty}, \quad a_2 = \frac{4}{5R_A^2}, \quad a_3 = 1-\frac{R_A}{R_\infty},$$

$$a_4 = -\frac{5}{2}(1-\alpha_2 R_A)R_A,$$

$$a_5 = \left(-1+1/R_\infty-\frac{3}{2R_A}\right)\left(a_6-\frac{28}{75}\right),$$

$$a_6 = -98/(-72+42R_A^{-1}+12R_\infty^{-1}).$$

Now we can plot the dependence of the exponent in equation (2) on the molecular Prandtl number. For both cases A2 (variants A2a and A2b) and B (variants B1 and B2), corresponding to Prandtl numbers $\sigma < 1$ and $\sigma > 1$, the exponent β is calculated as $\beta = \min(\beta_1, \beta_2)$, where the value of β_1 is determined by the rate of the function K' variation, and the value β_2 by the rate of the function d'.

Figure 1(a) plots the exponents β_1, β_2 and the resulting exponent β vs molecular Prandtl number together with the variation of the ratio R_A and of the asymptotic value of wave averaged mass flux q_A calculated according to relations (5) and (6). At $\sigma \to 1$ the exponent β tends to zero. At increase of σ starting from the point $\sigma = 1$ the value of R_A begins to differ from the value R_∞. At $\sigma \to \infty$ the value of R_A tends to about 0.15, and R_∞ to 0.2, so the ratio R_A/R_∞ tends to 3/4 (Fig. 1(a)). At $\sigma > 1$ the turbulent mass flow q_A is negative and attains the value of about $-68/15$ at $\sigma \to \infty$. The fact, that $q_A = 0$ at $\sigma < 1$ and $q_A \neq 0$ at $\sigma > 1$ means, according to the definition of q_A, that the difference of exponents in equation (2) for Q and $\hat{E}$ is less than unity at $\sigma < 1$, and is equal to unity at $\sigma > 1$.

Substituting the asymptotic limits R_A and q_A into the equation for TKE

$$\frac{t}{\hat{E}}\frac{\mathrm{d}\hat{E}}{\mathrm{d}t} = -\frac{2}{p}(\hat{R}^{-1}+\hat{q})$$

we obtain for the exponent β_E

$$\beta_E = -\frac{t}{\hat{E}}\frac{\mathrm{d}\hat{E}}{\mathrm{d}t} = \begin{cases} 5/2 & \text{at } \sigma < 1 \\ R_\infty(2+1/2R_A) & \text{at } \sigma > 1 \end{cases} \qquad (24)$$

At asymptotically large Prandtl number $\sigma \gg 1$ the values of R_∞ and σ_∞ are respectively equal to 0.2 and 0.164. The value of R_A is equal to 0.15 and the value of R_A/R_∞ to 3/4. So, the exponent in the power law of the TKE decay at $t \to \infty$ and $\sigma \to \infty$ is essentially less than the exponent 5/2 in the first line of equation (24) at $\sigma < 1$. The dependence of this exponent, β_E, is plotted against the Prandtl number, σ, in Fig. 1(b). At variance of σ in the range from 1 up to about 10 a smooth variance of β_E from 5/2 to unity occurs.

Appropriate to equation (24) the power law dependence for the TKE

$$E = E_0 t^{-\beta_E}$$

reveals (Fig. 2) a very good conformity with the numerical calculation of ref. [5]. The TKE components R_{11}, R_{22} and R_{33} decay with the same rate as E at $\sigma > 1$. In the final stage of decay E is determined,

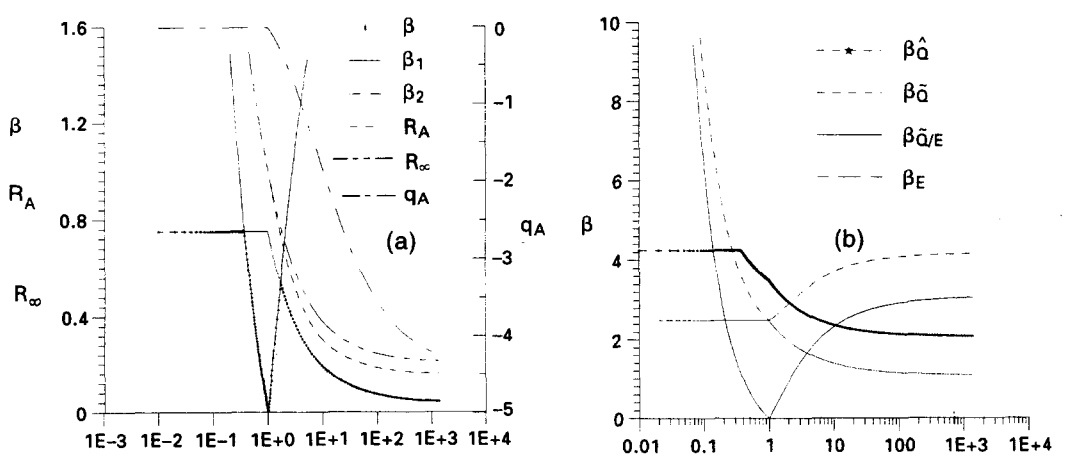

Fig. 1. Variation of the exponents with molecular Prandtl number σ: (a) variation of β_1, β_2, $\beta = \min(\beta_1, \beta_2)$, R_A, R_∞ and q_A; (b) variation of β_E, β_Q, $\beta_{\tilde{Q}/E}$, $\beta_{\tilde{Q}}$.

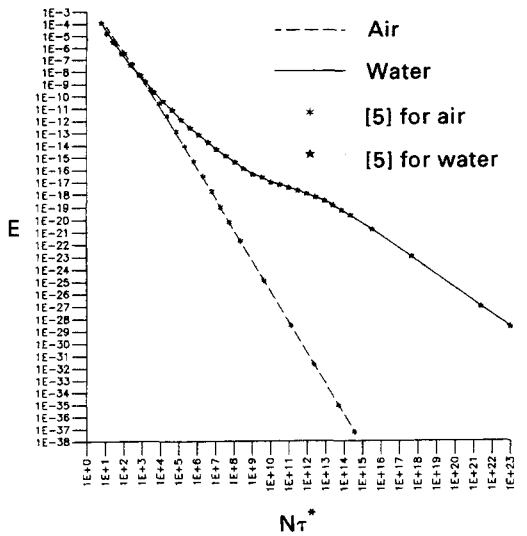

Fig. 2. Evolution of turbulence kinetic energy. Lines predicted according to equation (24); symbols numerically calculated in ref. [5].

mainly, by its vertical component R_{22}. The kinetic energy input from the potential energy of scalar field is distributed into the component R_{22}, from which it is redistributed into other components.

At $\sigma < 1$ the kinetic energy E and its component R_{22} decay with the different rates. The exponent in the power law for component R_{22} is equal to: $\beta_{R_{22}} = \beta_E + \beta_K$, where β_E is determined by equation (24), $\beta_K = \min(\beta_1, 3/4)$, and β_1 is given by expression (13). As $\beta_K > 0$, the component R_{22} decays faster than the turbulence energy itself. Accordingly, the fluctuation field becomes flat at $\sigma < 1$ in the final stage of decay and consists of the fluctuations in the directions of orts 1 and 3.

Differentiating the third equation in equation (3) and substituting the derivatives from system (1), we obtain

$$\hat{q} = \frac{(\hat{R}^{-1} - 1)(\hat{K} - 1)\hat{\vartheta}}{(1 + \hat{\vartheta})(2\hat{K} - 9/5)}.$$

This expression is a special case of expression (15) from ref. [6] at $d \to 1$ and $p_1 \to 0$. Using the relation $\hat{K} = \hat{\vartheta}/(\hat{\vartheta} + 1)$ which follows from $\hat{A}_1 = 0$ at $\hat{d} = 1$, one can exclude $\hat{\vartheta}$ from the last expression

$$\hat{q} = \frac{(\hat{R}^{-1} - 1)(\hat{K} - 1)\hat{K}}{(2\hat{K} - 9/5)}. \tag{25}$$

Relation (25) is universal to the variance of molecular Prandtl number as well as expression (15) from ref. [6], which is a rather good approximation for the case of air (Fig. 3(a)) not only in the final stage of decay, but also in the whole distant area. For the case of water (Fig. 3(b)) the agreement is worse due to a much slower tendency of the d-function to unity. It is proven by the comparison (Fig. 3) of dependencies (25) with the more general relation (15) from ref. [6]. Here, we should remember, that for air with the Prandtl number $\sigma = 0.73$ asymptotic variant A2b is realized, in which the function d' decays faster than the other functions in system (9). For salt-water with the number $\sigma \gg 1$ this function decays with the same rate, as the other functions.

In the case of water the power solution conforms with the numerical calculation only at $\tilde{\tau} > 10^{11}$ (see Fig. 3(b)). At the same time functional dependence, equation (6) is roughly valid for the whole distant

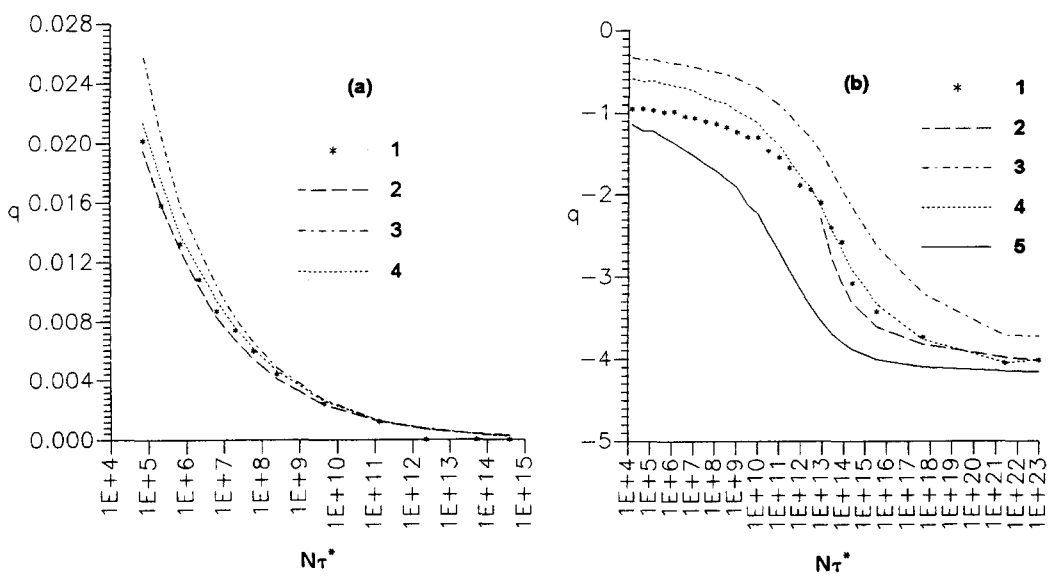

Fig. 3. Comparison of numerical results of ref. [5] for time evolution of the turbulent mass flow q (symbols) with analytical predictions (lines): (a) in the air case ($\sigma = 0.73$, $F = 2.64 \cdot 10^{-2}$); (b) in the water case ($\sigma = 800$, $F = 3.67 \times 10^{-2}$). 1—ref. [5]; 2—according to equation (2); 3—equation (25); 4—equation (15) from ref. [6]; 5—equation (6).

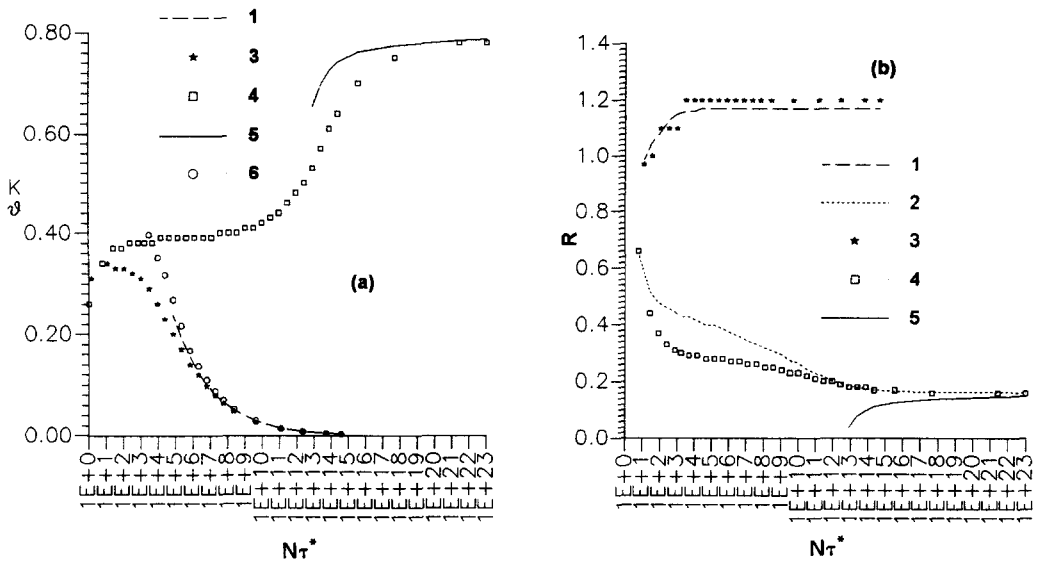

Fig. 4. Evolution of functions (a) K; (b) R. Lines—prediction; symbols from [5]: 1, 3—for air; 2, 5—for water; 1, 5—according to equation (2), 2—equation (20); 6—ϑ from ref. [5].

area, Fig. 3(b). For air the power solution corresponds to the numerical calculation rather well. The factor c_q in power dependence (2) was taken from the numerical solution at $t \to \infty$.

Having determined the factor c_q, it becomes possible to calculate (according to relation (16) for air and relation (23) for water) the values of coefficients c_i in power laws (2) for the other functions and to compare them with the numerical solution.

Figure 4(a) shows such a comparison for the function K, representing a part of vertical fluctuations in TKE. For air the conformity of power solution (2) (at β_K given by equation (14) and c_k by equation (16)) with the numerical calculation of ref. [5] is better, than for the water case, defined by formulae (2), (21), (23). For air in the final stage of turbulence decay the power solutions for the functions K' and ϑ' coincide each other, so numerical data for ϑ are also indicated.

The ratio $\vartheta/(\vartheta+1)$ represents the part of potential energy in total energy (potential plus kinetic), the ratio $1/(\vartheta+1)$—the part of kinetic energy. As easy to see, there is no fossilisation in a final stage of turbulence evolution at $\sigma < 1$, when $\vartheta \to 0$. At $\sigma > 1$ the ratio $\vartheta/(\vartheta+1)$ tends to 4/5. As it was pointed out in ref. [18] vertical mass flux $\overline{\rho w}$ is the best diagnostic tool for distinguish turbulence from waves, $\overline{\rho w}$ will have mean zero value for random internal wave free of turbulence fluctuations. Gerz and Schumann, [14], show at fossil states the vertical flux is not zero, $\overline{\rho w} \neq 0$, because of turbulent mixing occurring at low scales, $L_O \div L_K$. It was also pointed out in refs. [3, 15, 14] that fossilisation takes place only at $\sigma > 1$. Our analysis fully supports this point of view (see also plot of q_A in Fig. 1(a)).

The power law dependence $R(t)$ for air (Fig. 4(b)) practically coincides with the numerically calculated data. A small divergence is caused by the fact that the value of R was recorded in numerical file only with two significant figures. For water the conformity begins only since $\tilde{\tau} = 10^{15}$. The formula for asymptotic value of R_A, (20), has wider area of applicability.

Knowing the asymptotic limits for all the functions, it is easy to deduce the oscillation frequency and amplitudes in the final stage of decay.

From equation (19) at $d \to 1$ it follows for the frequency, ω, that

$$\omega^2 = 2(1+\hat{\vartheta})\left(\frac{9}{5}-2\hat{K}\right). \tag{26}$$

Expression (26) can be simplified, taking into account, that in a final stage $(1+\hat{\vartheta}) = (1-\hat{K})^{-1}$, so ω depend on $\hat{K}$ only

$$\omega^2 = \frac{2}{(1-\hat{K})}\left(\frac{9}{5}-2\hat{K}\right). \tag{27}$$

In the case $\sigma < 1$ the asymptotic value of ω^2 results in $\omega^2 = 18/5$, and in the case $\sigma > 1$—in $\omega^2 = 2$. Accordingly, the asymptotic limit of the oscillations period $T = 2\pi/\omega$ is equal to $\sqrt{10\pi/3} = 3.30$ at $\sigma < 1$ and to $T = \sqrt{2\pi} = 4.44$ at $\sigma < 1$ (see Fig. 5(a) from ref. [6]).

In ref. [3] the fossil turbulence was investigated by the DNS method. As earlier in ref. [17], DNS in ref. [3] started from ideal fossil conditions, that is from a field at rest with zero turbulence kinetic energy, but non zero potential energy of density fluctuations, $\vartheta_0 \neq 0$, $E = 0$; later the part of potential energy was transformed to kinetic energy during a wave-type process. The potential energy was converted at first into R_{22}-component and then redistributed to other components. In this regime R_{22} turns out to be larger than R_{11} and R_{33} ($K = R_{22}/E = 0.7$ in ref. [3], $K = 0.8$ in our analysis). Such distribution of TKE is in contrast

to that started from the initial conditions of another type, $\vartheta_0 = 0$, $E \neq 0$, [14], which leads to suppressing R_{22} component in a flow. In view of the fact that the oscillations in ref. [3] were masked by varying the averaged over the oscillation variables (those with hats in our analysis), the wrong conclusion was made concerning the noticeable variance of frequency. As it is easy to see, after deducing averaged over the oscillation values from the values presented in Fig. 1 from ref. [3], the period of oscillations turns out to be nearly constant, $N\tau^*/2\pi = 0.52$, $T = N\tau^* = 3.3$, coinciding with that of current analysis (see also Fig. 5(a) in ref. [6]). The value of $N\tau^*/2\pi \approx 0.5$ was pointed out in other theoretical investigations and numerical runs, see ref. [13]. In experimental works [2, 4, 9] the oscillations were also detected, but it was hard to determine their period in view of the necessity to have a very long tested section.

Unfortunately, we did not manage to do a more detailed comparison with paper [3] in view of the lack of information about time scales T_u and T_p in the initial field. Besides, the inverse Stanton number, St^{-1} in ref. [3], which is similar to the F^2 number in our dimensionless variables, was not small enough to be described by the perturbation theory developed.

The rate of the amplitude variance for the mass flux oscillation is dictated by expression (27) from ref. [6], taking $d' = 0$ in the final stage of decay, we can find

$$\beta_{\tilde{q}} = -\frac{t}{\tilde{q}'}\frac{\mathrm{d}\tilde{q}'}{\mathrm{d}t} = -\left[\frac{5}{2}\left(\frac{R_\infty}{R_A} - \sigma_\infty - \frac{3}{5}\right) + 5q_A R_\infty\right] - 1 \tag{28}$$

An analysis of expression (28) shows, that the exponent $\beta_{\tilde{q}}$ is equal to -1 at $\sigma = 1$. The negative value of $\beta_{\tilde{q}}$ does not contradict the physical sense, although it means an unlimited growth of the oscillations for $\tilde{q}$. Oscillations of Q and Q/E decay at any σ because the exponents, $\beta_{\tilde{Q}}$, $\beta_{\tilde{Q}/E}$ are always positive, as it will be shown below.

Let us compare the amplitude of the TKE oscillation, $\tilde{E}'$, with the mean value, $\hat{E}$, in a final stage of decay. The ratio $\tilde{E}'/\hat{E}$ can be estimated from the analysis made in ref. [6]. According to formula (25) from ref. [6], $\tilde{E}'/\hat{E} = 2\tilde{q}'/t\omega$. Considering the exponent in the power law of type (2) for the value $2q'/t\omega$ at $\hat{d}' \to 0$,

$$-\beta_{\tilde{q}/t} = \frac{t^2}{\tilde{q}'}\frac{\mathrm{d}(\tilde{q}')/t}{\mathrm{d}t} = \frac{t}{\tilde{q}'}\frac{\mathrm{d}(\tilde{q}')}{\mathrm{d}t} - 1$$

$$= p^{-1}\left[\frac{2}{\hat{R}} - \alpha_1 + 4\hat{q}\right] = \frac{5}{2}\left(\frac{R_\infty}{R_A} - \sigma_\infty - \frac{3}{5} + 2q_A R_\infty\right)$$

and substituting q_A from equation (25) one can show that the value $\beta_{\tilde{q}/t}$ is positive at any σ; so the ratio $\tilde{E}'/\hat{E}$ tends to zero at any molecular Prandtl number. The same is true for the ratio $\tilde{\vartheta}'/\hat{\vartheta} = -(2\tilde{q}'/t\omega)(1+\hat{\vartheta})/\hat{\vartheta} \to 0$, (at $\sigma < 1$ $\beta_{\tilde{\vartheta}/\hat{\vartheta}} = \beta_{\tilde{E}/\hat{E}} - \beta > 0$, at $\sigma > 1$ $\beta_{\tilde{\vartheta}/\hat{\vartheta}} = \beta_{\tilde{E}/\hat{E}} > 0$) as well as for the similar ratios $\tilde{K}'/\hat{K}$, $\tilde{R}'/\hat{R}$, $\tilde{d}'/\hat{d}'$.

Since, in the final stage the value of $\tilde{E}$ is small as compared with $\hat{E}$, we can write $\tilde{Q} = \tilde{q}E/t \cong \tilde{q}\hat{E}/t$, whence follows

$$\beta_{\tilde{Q}} = -\frac{t}{\tilde{Q}}\frac{\mathrm{d}\tilde{Q}}{\mathrm{d}t} = \beta_{\tilde{q}} + \beta_E + 1, \quad \beta_{\tilde{Q}/E} = \beta_{\tilde{q}} + 1. \tag{29}$$

Figure 1(b) plots the dependence (calculated from equations (28), (29) and (24)) of the amplitude rate exponents for appropriate functions vs the molecular Prandtl number σ. Here the exponent for $\hat{Q}$, β_Q, is calculated from the exponents for $\hat{q}$ and for $\hat{E}$, $\beta_Q = \beta + \beta_E + 1$ if $\sigma < 1$ and $\beta_Q = \beta_E + 1$ if $\sigma > 1$. The amplitude of $\tilde{Q}$-oscillations decays faster than the wave-averaged value, $\hat{Q}$, in the water case ($\sigma = 800$) and slower in the air case ($\sigma = 0.73$). Hence, in the final stage of decay a sine type dependence $Q(\tau)$ should be noticeably shifted on the plot. For the air case, this shift is very small as compared to peak values. In calculations of ref. [5] an opposite picture takes place (Fig. 22 from ref. [5]).

The reason for such a discrepancy probably lies in the inaccuracy of the account of amplitudes in ref. [5]. Really, it is impossible to carry out the calculations in equation (1) up to $\tilde{\tau} = 10^{22}$ and save the information on amplitude and phase of separate oscillation. It is known, that the oscillation period, T, is equal to about 3.5 units of $\tilde{\tau}$. Considering that for the proper calculation of oscillated functions it is necessary to have at least 20 time steps during a period; we can estimate a required number of time steps as $n = 20 \times 10^{22}/3.5$, that the computer is inaccessible for. Alternatively, in the calculations with very large time steps, averaged over oscillation values are obtained instead of true functions, as it has been shown above in Fig. 1(a) (b). As follows from relations (21)–(26) in ref. [6], all the amplitudes are proportional to the size of the amplitude $\tilde{q}'$, for which in ref. [6] a *differential* equation was obtained. Evidently, the value of $\tilde{q}'$ cannot be determined from the local values of wave-averaged functions. If after a great number of large steps in calculation one passes again to small ones with the aim to detect the oscillations, the algebraic relations between amplitudes should be obtained correctly, but the true value of amplitude $\tilde{q}'$ and so the true values of other amplitudes will be lost. For the proper analysis of the amplitudes in the far region it is necessary to add an additional differential equation for $\tilde{q}'$, equation (27) in ref. [6], to the considered model.

At the end of the given section we consider the postponed case, designated as A1, which corresponds to the Prandtl number $\sigma = 1$. In this case $q_A = 0$. $R_A = R_\infty = 1$, $\vartheta_A = K_A/(1-K_A)$, and the value of K_A remains uncertain. The analysis of this special case appears to be a little more complex, than of cases A2 and B. For instance, the asymptotic limit K_A can accept several possible values 0, 1/3, 9/10. Depending on the selected value of K_A the exponent β takes

different values. To select only one case we apply a continuity criterion for the dependence $\beta(\sigma)$ at $\sigma = 1$. From Fig. 1(a) it is clear, that at $\sigma = 1$ a zero value for β is natural. It corresponds to the trivial solution of system (8):

$$\beta_K = \beta_R = \beta_\vartheta = \beta_2 = 0, \quad \beta_d = 3/4,$$
$$q' = R' = \vartheta' = K' = 0 \tag{30}$$
$$K_A = 1/3, \quad q_A = 0, \quad \vartheta_A = 1/2, R_A = 1$$

and to a completely isotropic turbulence in the final stage of decay.

3. SCALE ANALYSIS

To understand better the essence of various modes we shall rely on scale analysis. To process experimental data in stratified flows the following length scales are usually introduced:

(1) $L_b = \overline{u_2^2}^{1/2}/N$ the buoyancy length scale characterized the largest turbulent scale which can be produced or maintained by buoyancy force. The part of the turbulence kinetic energy (TKE) contained in vertical velocity fluctuations, $\overline{u_2^2}$, is represented through this scale as $\frac{1}{2}\bar{\rho}N^2L_b^2$.

(2) $L_t = \overline{\rho^2}^{1/2}/(\mathrm{d}\bar{\rho}/\mathrm{d}x_2)$ the overturning or Ellison scale which is proportional to average deviation of density from its mean value $\bar{\rho}$. In other words, L_t is proportional to the displacement of fluid particles from their equilibrium level. This scale shows the level of existing potential energy due to density fluctuations $P = \frac{1}{2}\bar{\rho}N^2L_t^2$ and indicates predominant energy containing scale size. It is a convenient quality to measure.

(3) $L_O = (\varepsilon_u/N^3)^{1/2}$ the Ozmidov length scale at which buoyancy forces are equal to inertia forces. This scale is a buoyancy weighted turbulence dissipation rate. In fact, the Ozmidov scale is close to the largest possible turbulence scale allowed by buoyancy forces. If the integral length scale Λ_u or scale L_t is much less than L_b, the buoyancy does not affect the turbulence and the development of turbulence will mostly depend on the initial length scale ratio L_O/L_t. The Ozmidov scale is widely used in correlating experimental results on the collapse onset criteria ($\Lambda_u/L_O = 7$ according to ref. [10]), but it requires such a small value of the dissipation rate to be measured or estimated. This scale is of less importance in the region far from the turbulence source where wavefield motion dominates and estimations of dissipation rate might be suspicious. For the integral length scale Λ_u in the theory of ref. [7] the simple approximation $\Lambda_u = L_u/1 - d)$ was obtained.

In addition, Taylor microscales and macroscales for velocity and scalar field can be introduced in the ordinary way. Taylor microscales $\lambda_u = (5\nu\overline{u_i^2}/\varepsilon_u)^{1/2}$ and $\lambda_\rho = (6\kappa\overline{\rho^2}/\varepsilon_\rho)^{1/2}$ are considered as describing the average size of turbulence motion which determines dissipation processes, and Taylor macroscales $L_u = 5\overline{u_i^2}^{3}/\varepsilon_u$ and $L_\rho = 6\overline{u_i^2}^{1/2}\overline{\rho^2}/\varepsilon_\rho$ as describing the size of energy containing eddies. We suppose that in anisotropic flow these scales are still applicable at least for the turbulence in a horizontal plane.

Together with discussing length scales in a final stage of turbulence decay we shall compare these scales, calculated numerically according to turbulence model we use, with experiments at small and moderate values of $N\tau^*$, that is, in a region to which the majority of experimental data belong.

Helpful discussion regarding the scales L_b, L_t and their roles in stratified flow is contained in refs. [2, 4, 9]. The buoyancy length scale L_b is the scale for maximally possible overturning turbulent motion in a vertical plane. Turbulent scales are bounded by L_b, larger scales in vertical motion reveal themselves as internal waves. L_b is a source for L_t. Figure 5, where scales L_b and L_t are plotted against time, supports this point of view: phases of oscillations of L_b and L_t are opposite, after the onset of collapse L_b and L_t are linked together, L_t slightly exceeding L_b. Despite the fact that both scales, L_b and L_t, are closely linked, they behave differently in the initial region of the turbulent wake. In this region due to increasing potential energy at the expense of kinetic energy, L_b decreases as L_t grows (until $N\tau^* \approx 2$, see Fig. 5). During further development of the wake the viscous dissipation causes these scales to decrease with approximately the same rate, the ratio of L_t/L_b being constant.

The square of L_b/L_t represents the ratio of TKE closed in vertical fluctuations to potential energy of density fluctuations, $(L_b/L_t)^2 = K/\vartheta$. Equalling kinetic energy $\frac{1}{2}\overline{\rho w^2}$ and potential energy $\frac{1}{2}q(\partial\bar{\rho}/\partial z)^{-1}\overline{\rho^2}$ in gravity field one can obtain the criterion of pure wavefield motion as $L_b/L_t = 1$. In the final stage of turbulence decay this ratio was proven to be equal to 1 when $\sigma < 1$. In this case, as it was shown in previous section, $\overline{\rho w} = 0$. Oppositely, at $\sigma > 1$ the ratio L_b/L_t is equal to $L_b/L_t = \sqrt{1/5} = 0.447$ and $\overline{\rho w} \neq 0$. Both of these scales tend to zero at $t \to \infty$, $L_b/M = (KE/\varepsilon)^{1/2} \to 0$, $L_t/M = (\vartheta E/\varepsilon)^{1/2} \to 0$. At asymptotically large Prandtl number $L_b \sim L_t \sim t^{-8/15}$.

The calculated variance of the Ozmidov and Kolmogorov scales L_O and L_K in a homogeneous stratified flow is shown in Fig. 6 in comparison with experimental data. Here four experimental sets at different inverse Froude numbers F are presented, as well as two calculated curves corresponding to extreme large and extreme small F numbers in each set. A rather good degree of conformity especially in the water case was obtained. In the initial region $L_O > L_K$, further $L_O \sim L_K$ and then $L_O < L_K$ as the ratio $L_O/L_K = (ERe/T_u\varepsilon)^{3/4}$ constantly decreases. Full transition to waves (fossilisation) takes place at $L_O/L_K = 11$ [9]. Close criterion for this ratio was proposed in experiments in ref. [4], $L_O/L_K = 12.8$. According to ref. [1] the region $\Lambda_u \geqslant L_O > L_K$ corresponds to three-dimensional turbulence and the region $\Lambda_u \gtrsim L_O \sim L_K$ to so called two-dimensional turbulence in the horizontal plane combined with vertical internal waves.

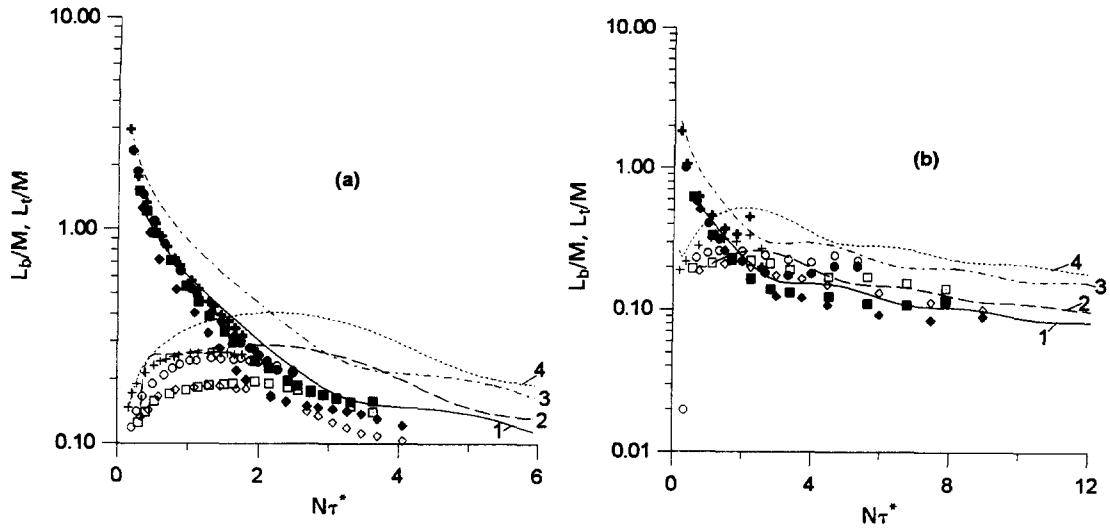

Fig. 5. Dimensionless scales L_b/M and L_t/M in theory (lines) and in experiment (symbols). (a) In conditions of ref. [2] in the air case: diamonds, 1, 2—$F = 0.0492$; squares—$F = 0.0441$; circles—$F = 0.0302$; plus, 3, 4—$F = 0.0236$. (b) In conditions of ref. [4] in the water case: diamonds, 1, 2—$F = 0.149$; squares—$F = 0.113$; circles—$F = 0.067$; plus, 3, 4—$F = 0.036$. Light symbols, 2 and 4—L_t/M; dark symbols, 1 and 3—L_b/M.

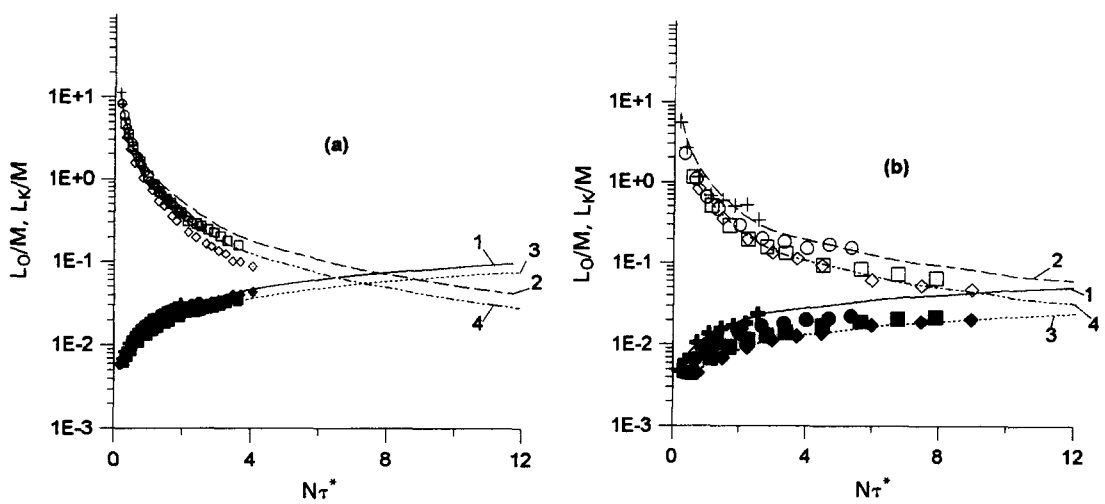

Fig. 6. Dimensionless Kolmogorov and Ozmidov scales L_K/M and L_O/M in theory and in experiment: (a) calculations for $F = 0.0492$ (1, 2) and for $F = 0.0236$ (3, 4) in the air case compared with the data of ref. [2]; (b) calculations in the water case for $F = 0.149$ (1, 2) and $F = 0.036$ (3, 4) compared with the data of ref. [4]. Light symbols, 2 and 4—L_O/M; dark symbols, 1 and 3—L_K/M. For symbol notation see Fig. 5.

Figure 7 plots the variance of the integral length scale Λ_u in stratified flow. As in previous figures comparison shows better agreement in the water case. In the air case the wavefield character of the integral length scale variance is essential in calculated results, but is very slight in experiments.

The ratio L_O/Λ_u is frequently used to estimate the collapse criteria. Oceanographic experiments show that at $L_O/\Lambda_u < 1$ the turbulence structure tends to be 2-D [1]. According to ref. [10] at the point of collapse onset $L_O/\Lambda_u = 1/7$. According to ref. [16] at this point $\Lambda_u/L_t = 1.25$. Collapse begins when $L_b/\Lambda_u = 1$ [1]. Full collapse occurs when $L_b/\Lambda_u = 0.2$–0.3. Figures 5–7 correspond to the foregoing results very well.

In many of the criteria proposed in the literature the overturning length scale L_t is compared with other turbulent scales. If $L_O/L_t \sim 1$ turbulent waves begins to dominate [1] (at $L_O/L_t < 0.7$ according to ref. [4]). Another criterion of fossilisation was suggested as the ratio L_b/L_t. If $L_b/L_t \gg 1$ (or $L_b/\Lambda_u \gg 1$) buoyancy does not take effect, the development will strongly depend on the initial conditions (mostly on the ratio L_O/L_t [4], if $L_O/L_t \gg 1$ this ratio will decrease and then the buoyancy will effect the turbulence). At the break

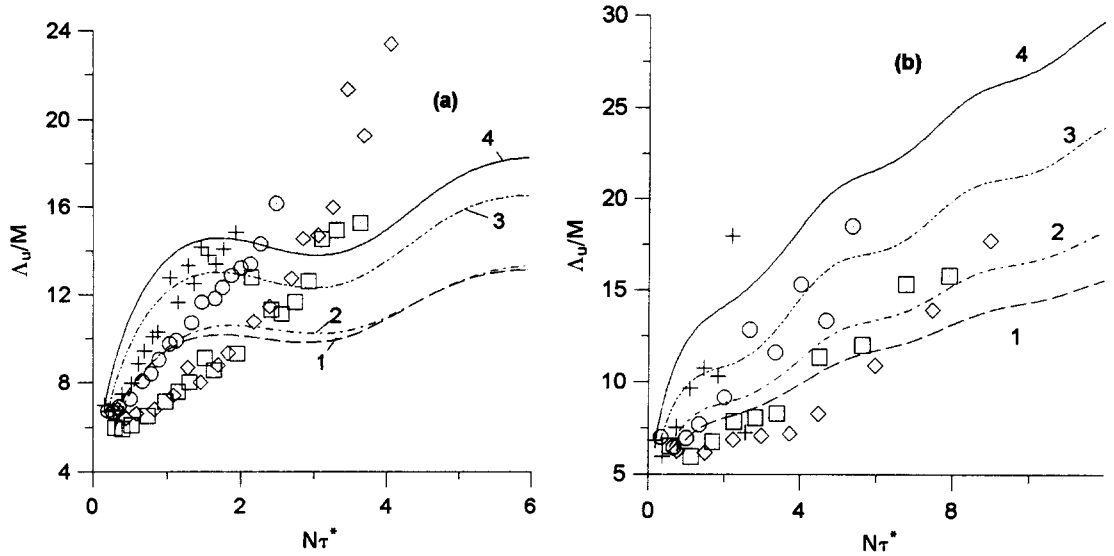

Fig. 7. Integral length scale in calculation (lines) compared with experiments (symbols) of ref. [2]: (a) 1, diamonds, $F = 0.0492$; 2, squares, $F = 0.0441$; 3, circles, $F = 0.0302$; 4, plus, $F = 0.0236$; and of ref. [4]: (b) 1, diamonds, $F = 0.149$; 2, squares, $F = 0.113$; 3, circles, $F = 0.067$; 4, plus, $F = 0.036$.

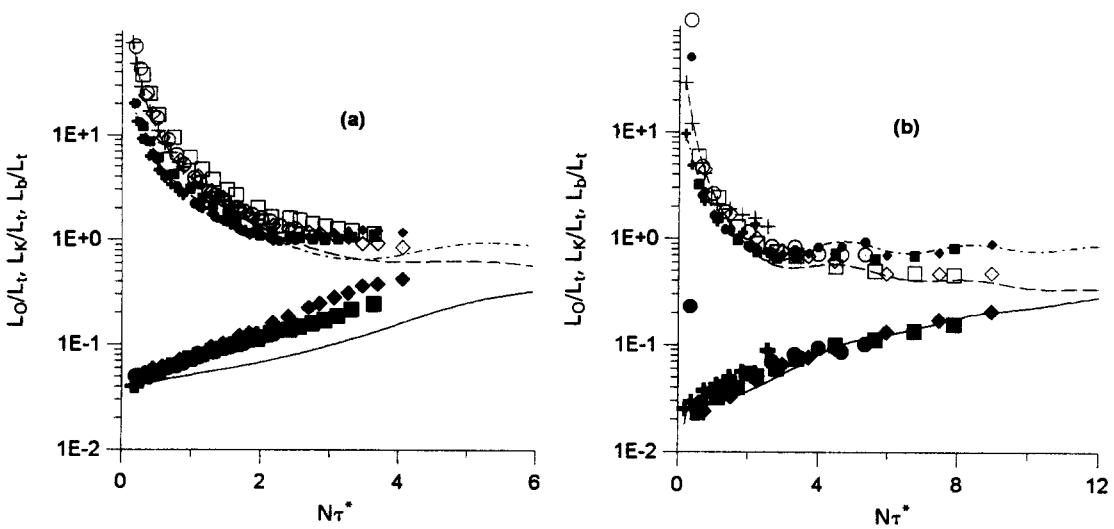

Fig. 8. Scale ratios L_O/L_t, L_K/L_t, L_b/L_t in theory (lines) and in experiment (symbols). (a) Comparison of calculations for $F = 0.0236$ in the air case with the data of ref. [2]; (b) comparison of calculations for $F = 0.036$ in the water case with the data of ref. [4]. Solid lines and large dark symbols, L_K/L_t, dashed lines and light symbols, L_O/L_t, dash-dotted lines and small dark symbols L_b/L_t. For symbol notation see Fig. 5.

point [4, 9, 10] $L_b/L_t = 1.25$, $L_O/L_t = 1.43$ independently of Re, active turbulence exists if $L_O/L_t \geqslant 1.25$ and $L_K/L_t \leqslant 0.14$. The calculated scale ratios L_O/L_t, L_b/L_t, L_K/L_t are plotted in Fig. 8. In both cases $\sigma < 1$ (Fig. 8(a)) and $\sigma \ll 1$ (Fig. 8(b)) in the collapsed state the ratio L_b/L_t sets at a level of 1. On the whole Fig. 8 looks more universal than previous figures and the degree of conformity between experimental and theoretical predictions is better.

The variance of the non-dimensional Taylor's microscale λ_u/M in experiments practically coincides with the numerical simulation (Fig. 9). A plot of Taylor microscale for the scalar field λ_t/M (Fig. 10) is qualitatively similar, but the slope of numerical curves is less, to a factor of about 1.7.

To describe the behavior of length scales in a final stage of turbulence decay let us consider their expressions through the main variables of the problem (summarized below).

$$\frac{L_b}{M} = \left(\frac{KE}{\varepsilon}\right)^{1/2} \sim t^{-(\beta_3+\beta_E)/2}$$

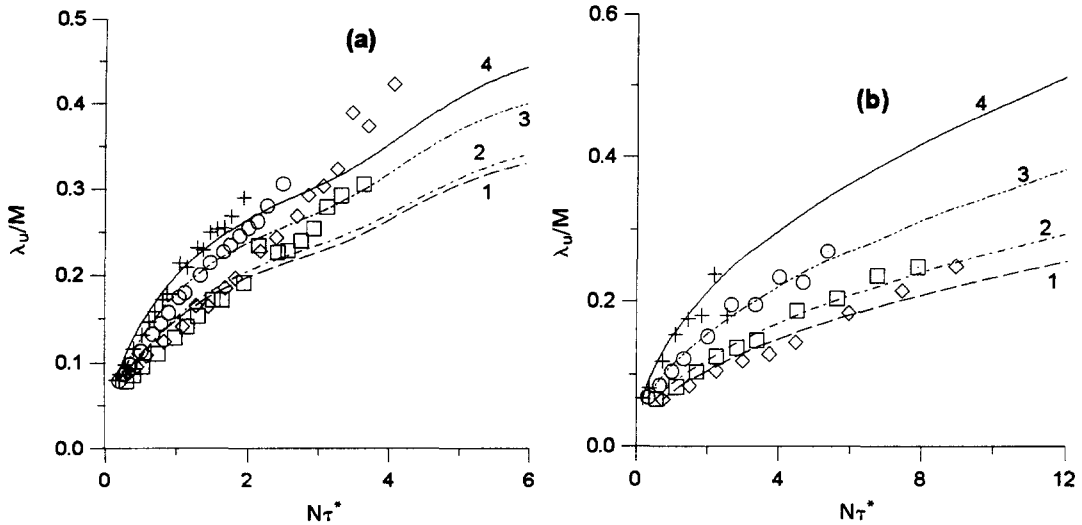

Fig. 9. Dimensionless Taylor microscale λ_u/M in theory (lines) and in experiment (symbols). (a) Comparison of calculations in the air case with the data of ref. [2]: diamonds, 1, $F = 0.0492$; squares, 2, $F = 0.0441$; circles, 3, $F = 0.0302$; plus, 4, $F = 0.0236$. (b) Comparison of calculations in the water case with the data of ref. [4]: diamonds 1, $F = 0.149$; squares, 2, $F = 0.113$; circles, 3, $F = 0.067$; plus 4, $F = 0.036$.

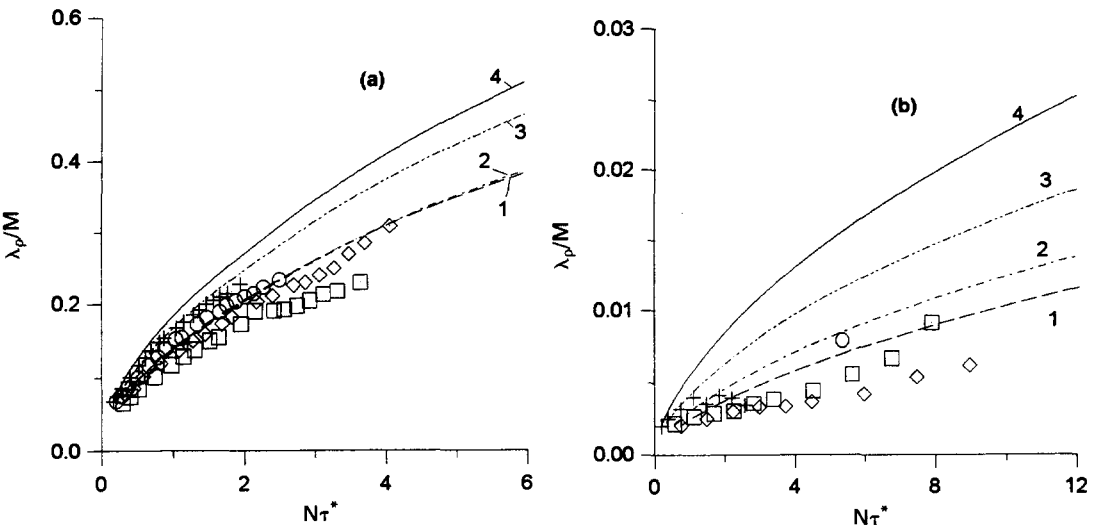

Fig. 10. Calculation of Taylor scalar field microscale (lines) compared with experiments (symbols) of ref. [2] (a): 1, diamonds, $F = 0.0492$; 2, squares, $F = 0.0441$; 3, circles, $F = 0.0302$; 4, plus $F = 0.0236$ and of ref. [4] (b): 1, diamond, $F = 0.149$; 2, squares, $F = 0.113$; 3, circles, $F = 0.067$; 4, plus $F = 0.036$.

$$\frac{L_t}{M} = \left(\frac{\vartheta E}{\varepsilon}\right)^{1/2} \sim t^{-(\beta_3+\beta_E)/2}$$

$$\frac{L_K}{M} = \left(\frac{T_u}{ERe^3}\right)^{1/4} \sim t^{(1+\beta_E)/4}$$

$$\frac{L_O}{M} = \left(\frac{E}{T_u F^3}\right)^{1/2} \sim t^{-(1+\beta_E)/2}$$

$$\frac{\Lambda_u}{M} = \frac{5E^{1/2}T_u}{1-d} \sim t^{-(\beta_E/2)+1+\beta_2}$$

$$\frac{L_u}{M} = 5E^{1/2}T_u \sim t^{-(\beta_E/2)+1}$$

$$\frac{L_\rho}{M} = 6E^{1/2}T_\rho \sim t^{-(\beta_E/2)+1}$$

$$\frac{\lambda_u}{M} = (5T_u/Re)^{1/2} \sim t^{1/2} \qquad \frac{\lambda_\rho}{M} = (6T_\rho/\sigma Re)^{1/2} \sim t^{1/2}$$

$$\frac{L_O}{L_t} = (\vartheta T_u F)^{-1/2} \sim t^{(\beta_3-1)/2} \qquad \frac{L_b}{L_t} = (K/\vartheta)^{1/2} \sim \text{const.}$$

$$\frac{L_K}{L_t} = \left(\frac{T_u F^3}{\vartheta^2 Re^3 E^3}\right)^{1/4} \sim t^{(1/4)+(2/4)\beta_3+(3/4)\beta_E}$$

where the exponent β_3 is derived as $\beta_3 = \beta$ at $\sigma < 1$ and $\beta_3 = 0$ at $\sigma > 1$. These expressions show the power laws for appropriate function at infinite time.

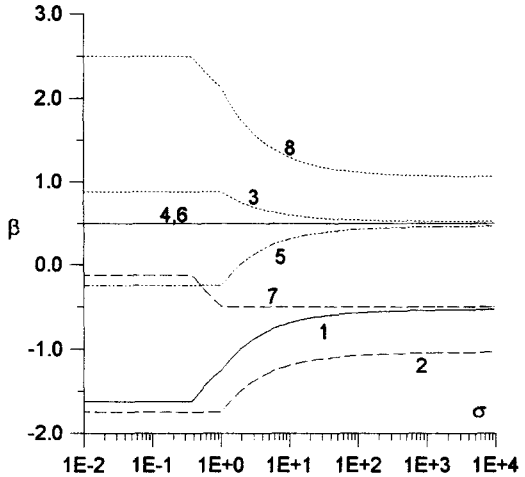

Fig. 11. The exponents in power laws vs Prandtl number. 1—β_{L_b}, β_{L_t}; 2—β_{L_O}; 3—β_{L_K}; 4—β_{Λ_u}; 5—$\beta_{L_u}, \beta_{L_\rho}$; 6—$\beta_{\lambda_u}, \beta_{\lambda_\rho}$; 7—$\beta_{L_O}/L_t$; 8—$\beta_{L_K}/L_t$.

The corresponding plot is built in Fig. 11. As was already mentioned, in a final stage two closely coupled scales L_b and L_t decay with the same rate (curve 1) exceeding the Ozmidov length scale L_O (curve 2). So, the ratio L_b/L_t is constant, the ratio L_O/L_t decreases (curve 7, see also Fig. 8). Taylor macroscales L_u and L_ρ decrease at $\sigma < 1.8$, but increase at $\sigma > 1.8$. Taylor macroscales usually describe the average size of energy containing vortexes in a turbulent flow. Large vortexes in a horizontal plane were observed in a number of visualizations of stratified flow (see review [1]). Laws of L_u and L_ρ variance probably correspond, to some extent, to the behavior of such large structures. Because of being two-dimensional in their nature, large vortexes do not affect the integral length scale substantially. The integral length scale Λ_u grows, as Taylor microscales λ_u and λ_ρ, with the exponent 0.5. It indicates that integral length scale is fully determined by dissipation processes. The Kolmogorov length scale L_K grows faster than Λ_u. Asymptotically, at very large Prandtl numbers σ the exponents for L_K, L_u, L_ρ are close to the universal exponent 0.5.

4. CONCLUSIONS

At the analysis of the final stage of turbulence decay the tendency of the functions K, R to different limits at $\sigma < 1$ and $\sigma > 1$ [5], is analytically justified. The dependence of these limits on molecular Prandtl number was obtained.

There are three cases, named in the work A1, A2 and B, distinguished by different asymptotic values of $\hat{K}$: 1/3, 0 and 4/5. These asymptotic limits are given by the expressions (4)–(7). The rates of tendency to the limits were investigated in the form of equation (2). On the basis of such an analysis we concluded that molecular Prandtl numbers $\sigma < 1$ correspond to the case A2, $\sigma > 1$—to the case B, and $\sigma = 1$—to the case A1.

Each of the cases A2 and B is subdivided into two asymptotic branches, A2a, A2b and B1, B2 with different rates of tendency to the limits. At increase of Prandtl number from zero up to unity the transition from the branch A2a to the branch A2b happens at $\sigma = 0.13$. For the branch A2a the exponents of tendency to the limits are identical for all functions and equal to $-3/4$. The coefficients at powers in equation (2) are given by the expressions (11)–(12). For the branch A2b these values are calculated from expressions (14) and (16), accordingly.

In case B the transition from branch B1 to branch B2 at an increase of Prandtl number occurs at $\sigma_{T2} = 1.7$, the exponent in expression (2) is calculated on the basis of equations (19) and (21), and the coefficients from equations (22) and (23).

It is shown, that the turbulence kinetic energy in density stratified media with molecular Prandtl numbers $\sigma < 1$ and $\sigma > 1$ decays under the different power laws, the exponent of decay is determined at $\tau \to \infty$ by expression (24). The turbulence kinetic energy degenerates at $\sigma > 1$, much slower than in the isotropic case due to a large part of this energy being enclosed in regular oscillation with weak attenuation. All asymptotic modes considered in the work and approximate analytical solutions are confirmed by the numerical calculation.

Acknowledgements—This work was supported, in part, by Soros Humanitarian Foundation Grant awarded by The American Physical Society.

REFERENCES

1. Hopfinger, E. J., Turbulence in stratified fluids. A Review. *Journal of Geophysical Research*, 1987, **92,** 5287–5303.
2. Lienhard, J. H. and Van Atta, C. W., The decay of turbulence in thermally stratified flow. *Journal of Fluid Mechanics*, 1990, **210,** 57–112.
3. Gerz, T. and Yamazaki, H., Direct numerical simulation of buoyancy-driven turbulence in stably stratified fluid. *Journal of Fluid Mechanics*, 1993, **249,** 415–440.
4. Itswiere, E. C., Helland, K. N. and Van Atta, C. W., The evolution of grid-generated turbulence in a stably stratified fluid. *Journal of Fluid Mechanics*, 1986, **162,** 299–338.
5. Kolovandin, B. A., Bondarchuk, V. U., Meola, C. and De Felice, G., Modelling of the homogeneous turbulence dynamics in stably stratified media. *International Journal of Heat and Mass Transfer*, 1993, **36,** 1953–1968.
6. Babenko V. A., Homogeneous turbulence evolution in stably stratified flow—I. Internal gravity waves at low inverse Froude numbers. *International Journal of Heat and Mass Transfer*, 1997, **40,** 1951–1961.
7. Kolovandin, B. A., Modelling the dynamics of turbulent transport processes. In *Advances in Heat Transfer*, 1991, Vol. 21. Academic Press, New York, pp. 185–234.
8. Van Dyke, M., *Perturbation Methods in Fluid Mechanics*, Academic Press, New York, 1964.
9. Stillinger, D. C., Helland, K. N. and Van Atta, C. W., Experiments on the transition of homogeneous turbulence to internal waves in a stratified fluid. *Journal of Fluid Mechanics*, 1983, **131,** 91–122.

10. Dickey, T. D. and Mellor, G. L., Decaying in neutral and stratified fluids. *Journal of Fluid Mechanics*, 1980, **99,** 13–31.
11. Nayfeh, A., *Perturbation Methods*. Wiley Interscience, New York, 1974.
12. Dunn, D. W. and Reid, W. H., Heat transfer in isotropic turbulence during final period of decay. NACA report TN4186, 1958.
13. Hunt, J. C. R., Stretch, D. D. and Britten, R. E., Length scales in stably stratified turbulent flows and their use in turbulence models. In *Stably Stratified Flows and Dense Gas Dispersion*, ed. J. S. Puttock. Clarendon, Oxford, 1988, pp. 285–321.
14. Gerz, T. and Schumann, U., Direct simulation of homogeneous turbulence and gravity waves in sheared and unsheared stratified flows. In *Turbulent Shear Flows*, Vol. 7. Spinger, Berlin, 1991, pp. 27–45.
15. Gerz, T., Schumann, U. and Elgobashi, S. E., Direct numerical simulation of stratified homogeneous turbulent shear flows. *Journal of Fluid Mechanics*, 1989, **200,** 563–594.
16. Metais, O. and Herring, J. R., Numerical simulation of freely evolving turbulence in stably stratified fluids. *Journal of Fluid Mechanics*, 1989, **202,** 117–148.
17. Gibson, C. H., Laboratory, numerical and oceanic fossil turbulence in rotating and stratified flows. *Journal of Geophysical Research*, 1991, **96,** 12549–12566.
18. Stewart, R. W., Turbulence and waves in stratified atmosphere. *Radiographic Science*, 1969, **4,** 1269–1278.